One-channel time reversal focusing of ultra-high frequency acoustic waves on a MEMS

Hatem Dahmani, Nikolay Smagin, P. Campistron, J. Carlier, Malika Toubal, Bertrand Nongaillard

Applied Physics Letters

RESEARCH ARTICLE | MARCH 07 2023

One-channel time reversal focusing of ultra-high frequency acoustic waves on a MEMS

H. Dahmani ; N. Smagin ; P. Campistron ; J. Carlier ; M. Toubal ; B. Nongaillard

Appl. Phys. Lett. 122, 102201 (2023)
https://doi.org/10.1063/5.0142179

Applied Physics Letters ARTICLE scitation.org/journal/apl

One-channel time reversal focusing of ultra-high frequency acoustic waves on a MEMS

Cite as: Appl. Phys. Lett. **122**, 102201 (2023); doi: 10.1063/5.0142179
Submitted: 12 January 2023 · Accepted: 20 February 2023 ·
Published Online: 7 March 2023

H. Dahmani, N. Smagin,[a] P. Campistron, J. Carlier, M. Toubal, and B. Nongaillard

AFFILIATIONS

Univ. Polytechnique Hauts-de-France, CNRS, Univ. Lille, UMR 8520 - IEMN - Institut d'Electronique de Microélectronique et de Nanotechnologie, F-59313 Valenciennes, France

[a]Author to whom correspondence should be addressed: nikolay.smagin@uphf.fr

ABSTRACT

This Letter reports on a work performed to fabricate and characterize a silicon micro-machined cavity dedicated to micro-resolution Ultra-High Frequency imaging in microfluidics and microbiological applications using one-channel time reversal. Time reversal provides the means to spatially and temporally localize elastic energy on a receiver. Here, the arrays of zinc oxide micro transducers are coupled with a 400 μm thick silicon wafer containing micromachined structures for acoustical field confinement. Characterization of the diffused acoustic field and time-reversal retro-focusing are reported. The transducers are wideband in the 0.2–2 GHz range with a central frequency of 0.9 GHz.

Time Reversal (TR) is based on the use of reciprocity and time reversal invariance of the wave equation.[1] In particular, time-reversed acoustics[2,3] (TRA) provides unprecedented possibilities for ultrasound (US) imaging,[4–7] medical ultrasound,[8,9] communications in complex media,[10–12] and nondestructive evaluation (NDE).[13–16] Initially, TR focusing (TRF) was considered with the use of multi-element phased array transducer able to record an acoustic field over extended spatial regions. Later, a one-channel TR was introduced as a low-cost technique able to focus acoustic energy anywhere[17,18] even on a 3D domain,[19] with a spatiotemporal resolution comparable to that of multiple transducer array.[4,20–22] Implementation of this technique requires a multi-reverberating regime that could be obtained by confining an ultrasonic field in an ergodic structure called a chaotic cavity.[18] Thus, the loss of spatial information is compensated by increased temporal information.

The reported TRA devices operate in the medical or the NDE frequency range (0.1–10 s MHz), and their spatial resolution is of the order of wavelength. Additionally, TR sub-wavelength focusing and super-resolution imaging could be achieved using phononic crystals and acoustic metamaterials.[5] For homogeneous media, exploiting TRF capabilities in the micrometric scale necessitates shifting the operating frequency toward the ultra-high frequency (UHF) range.

This Letter reports a feasibility of one-channel TRF of UHF (0.2–2 GHz) acoustic waves in the MEMS context. The overall device size is about $2 \times 2\,\text{mm}^2$; an acoustic reverberating medium was obtained by micromachining a standard silicon wafer. Integrated Zinc oxide (ZnO) transducers were used as emitters/receivers. The presented MEMS prototype is intended to provide a space-resolved measurement option for characterization techniques in the microfluidics domain, such as measurement of microdroplets viscosity,[23] mixture concentration,[24] wetting,[25] and others. As the authors are aware, this is the first implementation of acoustic UHF TR of acoustic waves. Earlier, the UHF range has been explored for TRF of electromagnetic waves.[26]

Figure 1(a) gives an overall schematics of the MEMS for TR imaging. The main structural element of the device is a 400 μm thick double-side polished silicon wafer of (110) crystalline orientation. The ergodic and chaotic ultrasound propagation was obtained by introducing irregularities using anisotropic wet etching [Fig. 1(b)]. The etched structures were represented by 220 μm height truncate pyramids whose lateral sides were inclined by 54.7° relative to their base (base dimensions are of order $1000 \times 1000\,\mu\text{m}^2$). Such an approach gave a possibility to obtain a diffused acoustic field in the partially confined region (leaky cavity)[22,27] surrounded by etched volumes [shown with red highlighting in Figs. 1(b) and 1(c)]. Due to the partial confinement, the diffused acoustic field could be observed in the region of the mentioned leaky cavity as well as outside of it. Two receiving transducer arrays referred to as $R_{i,j}$ and R_k were placed on the opposite side of the wafer, in the regions inside and outside the confined zone, respectively. The emitter E was situated in front of the inclined mirror to enhance multiple reflections [Figs. 1(a) and 1(b)]. The piezoelectric transducers were made of Zinc Oxide (ZnO). They had a diameter of 100 μm and

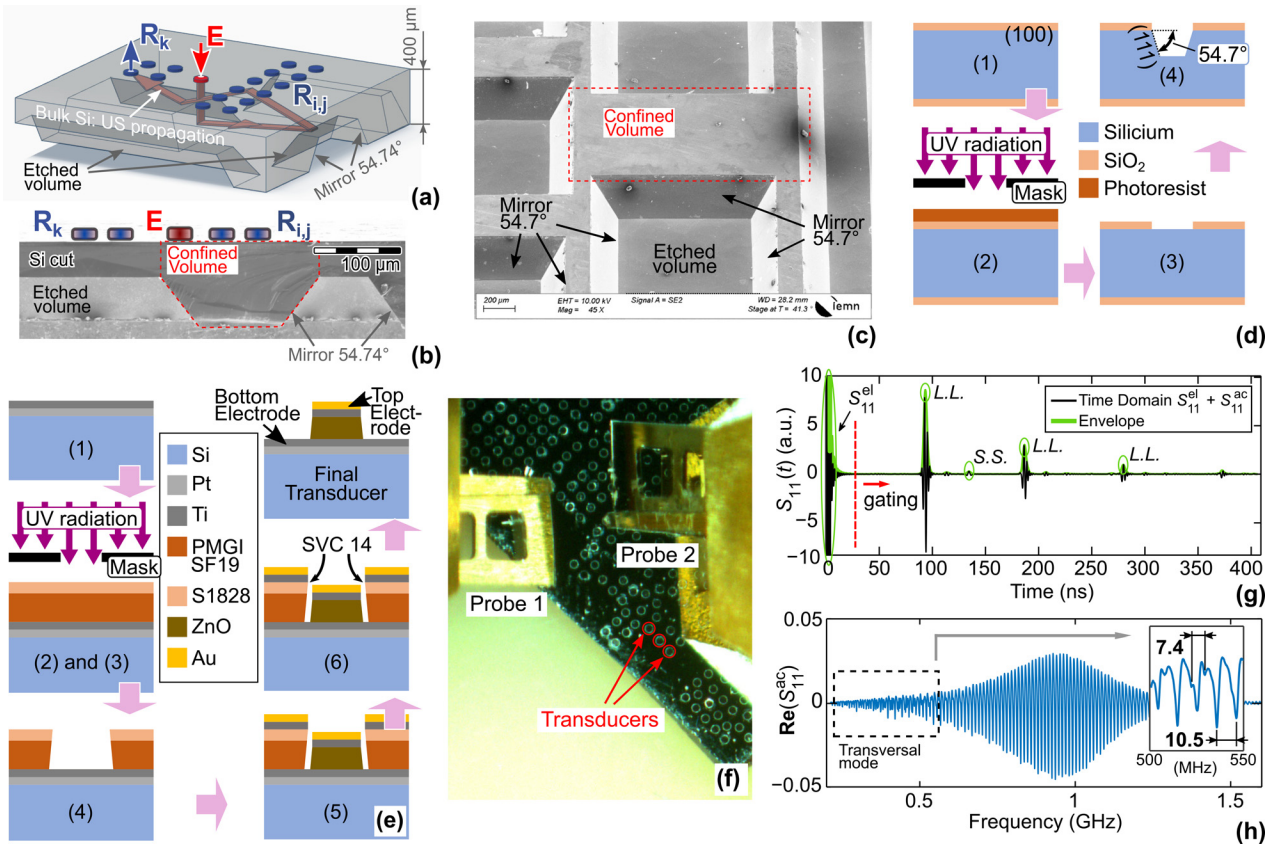

FIG. 1. (a) Schematic representation of UHF ultrasound TRF on a MEMS (E is a piezoelectric emitter, and $R_{x,y}$ are receivers). (b) SEM side-view of the etched silicon wafer. (c) SEM bottom-view of etched (110) Si wafer showing the zone of partial acoustic field confinement. (d) Technological steps for leaky cavity fabrication. (e) Technological steps for ZnO transducer fabrication. (f) Transducers' characterization using manual RF probes station and VNA. (g) Time domain signal of the full transducer reflection coefficient S_{11}. (h) Real part of S_{11}^{ac} in the frequency domain.

a thickness of 2 μm. The receiving transducers $R_{i,j}$ and R_k were spaced with a 190 μm pitch.

The starting phase of the MEMS fabrication consists in introducing irregularities in ultrasound propagation media.[28] In the first step of the anisotropic wet etching [1 in Fig. 1(d)], two 1600 nm layers of silicon oxide (SiO_2) were produced by thermal oxidation on both sides of the Si wafer. The oxidation was carried out at a high temperature (900–1000 °C) in water vapor (H_2O). After step 2 in Fig. 1(d), the SiO_2 layer was locally etched with hydrofluoric acid (HF) via a 2 μm thick positive photoresist mask (PMGI SF19 from Microchem Corporation and S1828 from Shipley Corporation) aligned in the ⟨110⟩ direction. The photoresist was then eliminated with acetone. Furthermore, in the third step, the silicon patterns were etched through the SiO_2 mask with 20% potassium hydroxide (KOH) at 80 °C. The etching is performed in the {111} plane at approximately 73 μm/h. Since the KOH wet etching is anisotropic, the etching rates are not equal for different crystal directions resulting in 54.7° lateral flanks inclination relative to the ⟨110⟩ Si plane[29] [step 4 in Fig. 1(d)]. This inclination is visible in the SEM image in Fig. 1(b). Figure 1(c) presents several neighboring etched pyramids dedicated to acoustic propagation confinement. Low intrinsic acoustical attenuation of silicon and high reflectivity of etched walls contribute to establishing long propagation paths and multiple reflections of acoustic waves.[30]

The MEMS fabrication's second phase consists of integrating the ZnO piezoelectric transducer array on the rear face of the substrate [Fig. 1(e)]. The process began with the deposition of the lower electrode, consisting of two layers: 10 nm of the titanium adhesion layer and 80 nm of the platinum conductive layer [step 1 in Fig. 1(e)]. A photolithography process was then performed to make the transducer's pattern, where a thick 8 μm layer of PMGI SF19 was dispensed by spin coating on the lower electrode. Furthermore, a layer of 1.5 μm of S1828 was appended (step 2). After ultraviolet exposure using a mask (step 3), a commercial developer MF 319 (Microposit) was used to obtain a pattern of 100 μm diameter circular transducers in the PMGI layer (step 4). Next, a 2 μm thin ZnO layer was deposed (step 5). Finally, 10 nm of titanium adhesion layer followed by 400 nm of gold was deposited. The last step is the lift-off process using SVC 14 (Shipley Corporation), where the UV-exposed resin is removed.

Photography of the micromachined transducer array can be seen in Fig. 1(f). The transducer electrical response was measured with a manual radio frequency (RF) probe station connected to a Vector Network Analyzer (VNA) Tektronix TTR 503. The used RF probes

(|Z|-Prob from Cascade Microtech with a 1250 μm pitch) were flexible enough to assure simultaneous electric contact with the transducer's top and bottom electrodes. The characterization measurement was carried out on a silicon wafer with no etching to reveal the response features related to the transducers only. Figures 1(g) and 1(h) reveal the S_{11} parameter measurement performed for one of the transducers in the time and frequency domain, respectively. In a frequency domain, it can be decomposed into two contributions as follows: $S_{11} = S_{11}^{el} + K_{11}S_{11}^{ac}$. Here, S_{11}^{el} is the reflection of the electromagnetic wave on the transducer due to a non-perfect electrical matching, S_{11}^{ac} represents all the acoustic wave reflections on the opposite side of the substrate converted into an electrical signal, and K_{11} is the electro-acoustic-electrical coupling coefficient of the ZnO transducer.

In the time domain, S_{11} signal is obtained with inverse Fast Fourier Transform (FFT). The electrical term S_{11}^{el} response appears shortly after the transducer's excitation. In contrast, the group of acoustic terms arises later [Fig. 1(g)]. The crystal orientation of the ZnO was intentionally set to be not perfectly vertical. That favored the generation of acoustic shear waves (SS), seen in the waveform among the longitudinal wave echoes (LL).[31] The acoustic-only transducer response can be obtained by gating the time domain signal after approximately 25 ns and performing the FFT. The resulting curve of real S_{11} part in Fig. 1(h) also reveals the presence of the transversal mode. The observed echoes correspond to the different acoustic signals traveling back and forth in the silicon wafer. They are separated by periods of 10.5 MHz for longitudinal waves and 7.4 MHz for shear waves [inset in Fig. 1(h)], defined by the Si wafer's double thickness (800 μm) and propagation velocity of the corresponding wave component ($V_L = 8432$ and $V_S = 5843$ m/s, respectively). In conclusion, the ZnO transducer's response shows that the latter can produce both longitudinal and shear waves in the ≈2 GHz range with a central frequency of 0.9 GHz for longitudinal waves.

The magnitude of mechanical displacement provided by ZnO transducers was measured by a Polytec UHF-120 laser Doppler vibrometer (LDV). The transducer was driven with a continuous sinusoidal signal by a Marconi 2030 RF generator connected to a power amplifier (Amplifier Research 50W1000A). The power of the electrical signal applied to the transducer was about 10 W. It was determined by the electrical breakdown limit of the 2 μm thick ZnO. The excitation signal was swept around a central frequency of 0.9 GHz with a 105 MHz span. Optical measurements were carried out in the frequency domain using the "peak hold" mode. As a result (Fig. 2), the measured displacement magnitude is about 25 pm. The mechanical behavior exhibited by the transducer is wideband and relevant to its electrically measured S_{11}^{ac} response [Fig. 1(h)]. The noise level of the vibrometer acquisition for time domain measurements is of the same order (20 pm) as the response for quasi-continuous excitation detected in a frequency mode. Furthermore, the displacement level provided by the ZnO transducer is considerably lower using pulsed excitation necessary for TRF. For this reason, time domain measurements with pulsed excitation (0.2–2 GHz linear chirp) were unsuccessful as the signal amplitude stayed below the mentioned noise level. In summary, the obtained displacement level was insufficient for TRF using vibrometer measurement, and the TR results reported below were obtained by electrical acquisition with arrays of receiving transducers.

One of the micromachined regions allowing acoustic field confinement is shown in Fig. 3(a). The central part possessing the initial

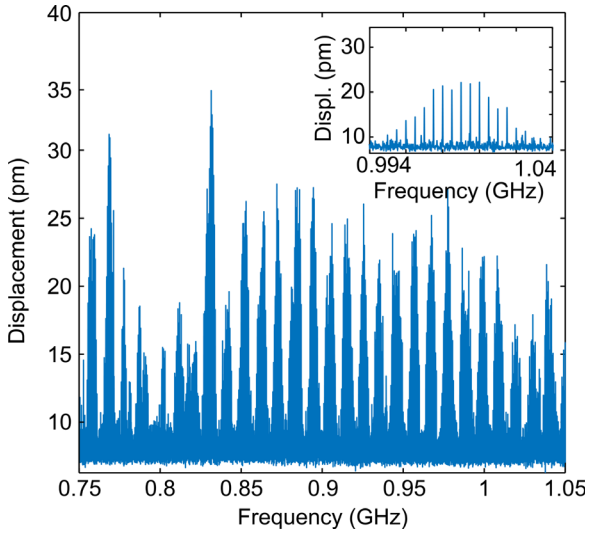

FIG. 2. Mechanical response of the ZnO transducer measured with a laser Doppler vibrometer directly on its surface.

layer thickness of 400 μm is surrounded from four sides with etched volumes. An emitter E is placed in front of the lateral mirror to reinforce multiple reflections. The internal volume of the leaky cavity is referred to as "Zone A" in Fig. 3(a) and in the sectional view S in Fig. 3(b). The "Zone A" area is 1480 × 720 μm^2; it contains an array of receivers $R_{i,j}$ $(i = 1, 2;\ j = 1\ldots6)$ placed to characterize the acoustic wave propagation. Another receiver array R_k $(k = 1\ldots4)$ is placed in one of the zones outside the leaky cavity referred to as "Zone B" in Figs. 3(a) and 3(b).

The impulse responses between the emitter and receivers were obtained with inverse FFT of the $S_{12}(f)$ measurements carried out on the RF probe station mentioned above [Fig. 1(f)]. As an example, the $S_{12}(f)$ signal between the emitter and the R_2 receiver from the "Zone B" is presented in Fig. 3(c). The observed features reveal the presence of diffused field: several ballistic arrivals at the beginning of the signal, increasing wave mixture, and exponentially decaying coda "tail" starting at $t_0 = 0.83$ μs. The estimated decaying rate linked with the attenuation in bulk Si is of 22 dB/μs. Thus, the coda signal is observable during approximately 1 μs, which contains about 900 periods at the central transducer frequency of 0.9 GHz. Such attenuation level might be sufficient for one-channel TR.[7]

Ergodic properties of the media could be verified using cross correlation analysis. Figure 3(d) presents the matrix of normalized cross correlation coefficients between all considered receivers. The correlation between noisy-like coda signals propagating in zones "A" and "B" is rather low, being within the range from −30 to −20 dB. Additionally, the correlation between the signals received in zone "B" is rather low as well, staying within limits from −25 to −15 dB. On the contrary, several elevated values of the coefficient (from −10 to −5 dB) could be observed for adjacent receivers in zone "A." This observation indicates that using zone "B" external to the leaky cavity could be preferable due to better ergodicity.

The presented MEMS allowed one-channel TR focusing of UHF ultrasonic waves. This goal has been achieved with the experimental setup presented in Fig. 4(a), which consisted of excitation (arbitrary

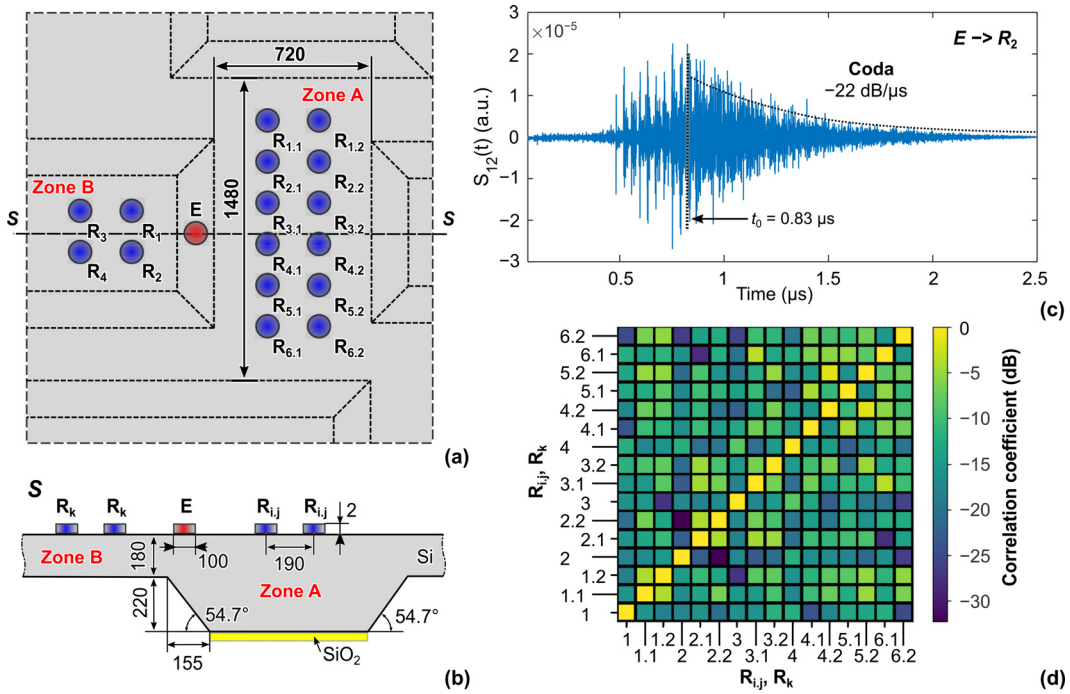

FIG. 3. (a) Scheme of a field confinement region and disposition of the ZnO transducers. (b) Side view S of the upper figure. (c) Impulse response $S_{12}(t)$ between E and R_2. (d) The cross-correlation coefficients for the total of considered receivers.

waveform generator Tektronix AWG 70002A) and acquisition (digital phosphor oscilloscope Tektronix DPO 71254C) units connected via Ethernet to a personal computer (PC). To improve the quality of spatiotemporal energy focusing, we used a linear chirped signal $S(t)$ for emitter excitation.[20,32] The 0.2–2 GHz linear up chirp was synthetized at 12.5 Gs/s, had a duration of 0.5 μs, and an amplitude of 0.5 Vpp. The received signals $R(t)$ were digitized by the oscilloscope at the same rate of 12.5 Gs/s during 4 μs.

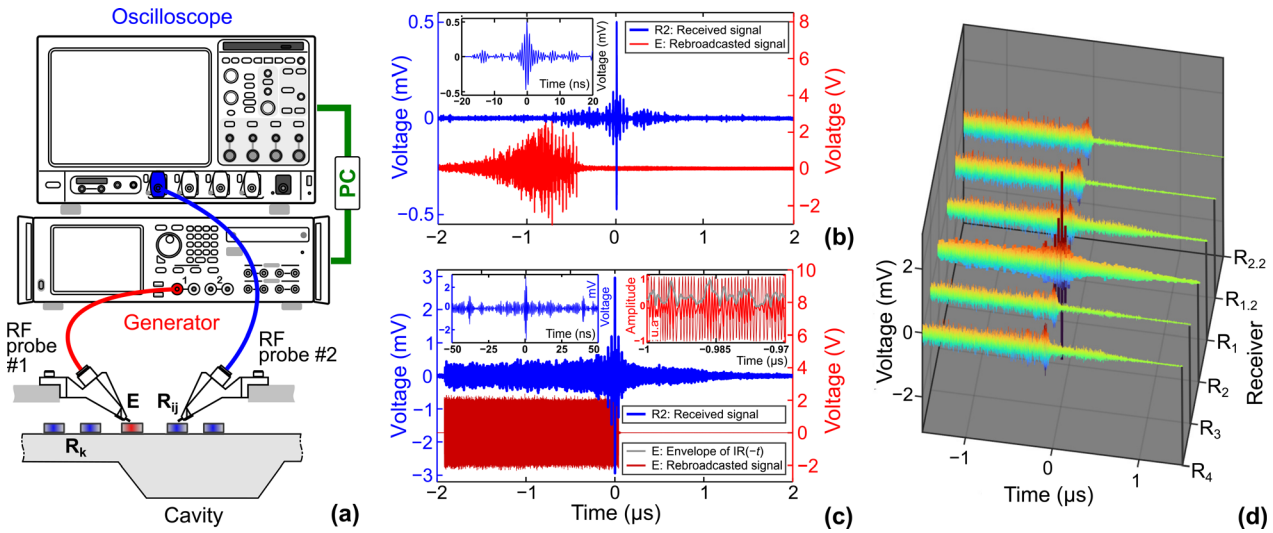

FIG. 4. (a) Experimental setup for one-channel spatiotemporal focusing with TR. (b) Time-compressed signal (blue) on R_2 using deconvolution and the rebroadcasted time-inversed impulse response (red); the central peak is zoomed on the inset. (c) The same time-compressed signal (blue) using deconvolution and envelope normalization of impulse response (red); the inset in the top-left zooms in on the central peak; the inset in the top-right illustrates the normalization procedure. (d) Simultaneous signal reception by an array of transducers while focusing on R_2 using impulse response normalization.

We implemented a reciprocal TR focusing using deconvolution[33,34] (or inverse filtering) procedure consisted of (i) recording the response for the chirped excitation $R(t)$; (ii) reconstructing propagation media impulse response (IR) by cross-correlating the chirp source $S(t)$ with the received signal from the chirp: $IR(t) = R(t) \circledast S(t)$; and (iii) rebroadcasting by the emitter E of the time-reversed impulse response $IR(-t)$. A full deconvolution comprising the acasual part has been used.[35,36]

The corresponding time-compressed signal received by R_2 is shown in Fig. 4(b) with the blue curve, while the red one depicts the rebroadcasted $IR(-t)$. The peak amplitude for a 250 mV_{0-p} excitation is 0.5 mV. Its width is 0.72 ns, which corresponds to $\approx$ 1.4 GHz. The presence of distinguishable periodic peaks on the impulse response and rather high sidelobes level (11.2 dB) indicate that the degree of the cavity's symmetry is still high.[37,38] The peak-to-noise factor is 21.5 dB.

The peak amplitude can be increased by implementing such procedures as 1-bit TR[39,40] or normalizing the $IR(-t)$ by its envelope. We implemented the latter technique and achieved a $\times 6$ enhancement up to 3 mV level [Fig. 4(c)]. In turn, this introduced some asymmetry and decreased the sidelobe ratio (8 dB), as well as peak-to-noise factor (14.8 dB). The duration of the retransmitted signal is 2 μs; the recompression peak appears almost at the end of the emission, preceded by an uncorrelated noise-like part (0.42 mV level). After the focal peak, the signal rings out within less than 2 μs.

The best theoretically achievable spatial resolution is of the order of one wavelength.[7] For the given central frequency of 0.9 GHz, the spatial resolution is of 10 μm order, which is significantly smaller than the spacing of the receivers (190 μm). As mentioned above, the ultrasound vibrations level was insufficient for optical measurement of the acoustic field on the MEMS surface, so the direct estimation of the spatial compression was not possible. However, the presence of spatial compression can be confirmed by simultaneous reception by the arrays R_{ij} and R_k. To this end, Fig. 4(d) shows a 3D waterfall plot containing signals received by the R_k array and arbitrarily chosen R_{11} and R_{22} from R_{ij}. The focalization is effectuated on R_2 with normalized $IR(-t)$. Only this channel exhibits a recompression peak. All other signals contain only the uncorrelated noise-like parts preceding the peak for R_2. The distribution of the non-compressed field is uniform within the studied region.

In order to characterize the amount of temporal focusing, we used the temporal compression ratio $\xi_t = E_F/E_T$, where E_F is the energy in the main peak of the TR signal, and E_T is the total signal energy.[35,41] ξ_t shows the amount of energy that is within the focal region (referred to as "Focal Energy" in Fig. 5) as opposed to the amount of energy that remains outside of that time interval ("Total Signal" in Fig. 5). The ratio should approach 1 for perfect focusing. The double duration of the rebroadcasted IR is used (4 μs) to let the signal ring out and calculate E_T.

We consider the TR signals at R_2 as in Figs. 4(b) and 4(c) to calculate ξ_t. For the time compression using deconvolution, $\xi_t = 29.6\%$, which is relevant to other data found in the literature for a lower frequency range.[35] As observed, ξ_t becomes lower for TR focusing using normalized IR, decreasing to 7.8%.

In conclusion, we have shown the feasibility of focusing UHF (0.2–2 GHz) ultrasounds in the MEMS context with a single ZnO micro-transducer coupled to a silicon wafer and using the deconvolution TR process. Measurements revealed that TRF is stronger in the zone external to the leaky cavity ["Zone B," Fig. 3(b)] compared to the internal cavity volume[22,27] ("Zone A"). In this case, the latter acts as a resonator with a weak quality factor and a strong leakage. In the future work, we plan to introduce more complex geometries (such as circular patterns) to increase ergodicity and minimize the sidelobes.

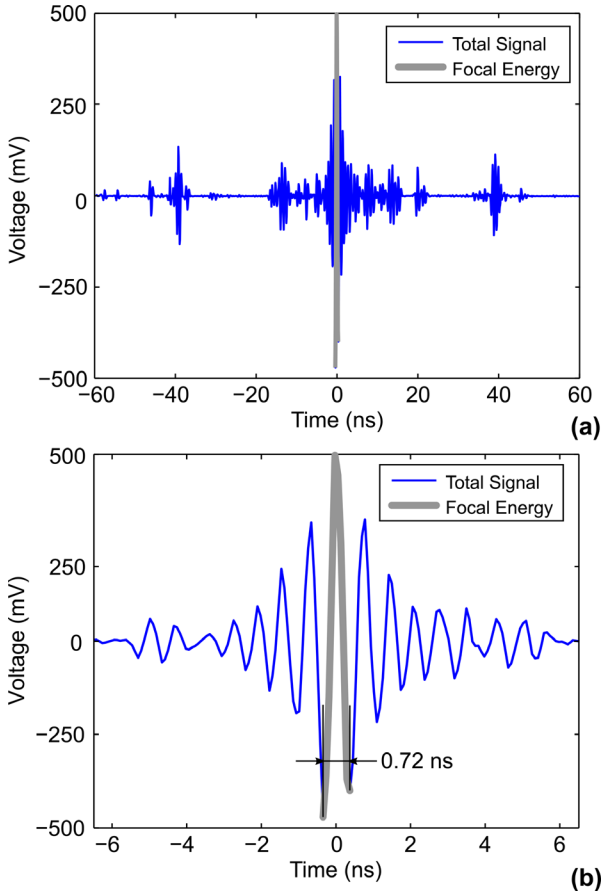

FIG. 5. Calculating the compression ratio for signal on R_2 obtained using deconvolution. (a) Ratio of the energy in the main peak to the total energy. (b) Zoom of the central peak.

The focusing "library" of impulse responses was recorded by an array of UHF transducers identical to the receiver. For imaging purposes, ideally, the formation of the "library" should be effectuated with LDV scanning. However, we used ZnO receivers because of the emitter limitation in provided vibrations level. Integrating an emitter with a higher electromechanical coefficient, such as a thin film of X-cut $LiNbO_3$, could achieve higher mechanical displacements, thus enabling optical measurements. Overall, the presented study presented a proof-of-concept of TRF of UHF ultrasonic waves and paved the way toward a real-time acoustic echographic sensor at a micrometric scale.

The research leading to these results has gratefully received funding from the French Government and the Hauts-de-France Regional Council. The authors acknowledge the cleanroom and characterization laboratory staff. This work was partly supported by

the French RENATECH network with the IEMN CMNF technological facilities.

AUTHOR DECLARATIONS

Conflict of Interest

The authors have no conflicts to disclose.

Author Contributions

Hatem Dahmani: Conceptualization (equal); Formal analysis (equal); Investigation (lead); Methodology (lead); Software (equal); Visualization (lead); Writing – original draft (lead); Writing – review & editing (lead). **Nikolay Smagin:** Conceptualization (supporting); Formal analysis (equal); Investigation (lead); Methodology (lead); Software (lead); Visualization (lead); Writing – original draft (lead); Writing – review & editing (lead). **Pierre Campistron:** Conceptualization (lead); Data curation (lead); Formal analysis (lead); Funding acquisition (lead); Investigation (supporting); Methodology (supporting); Project administration (equal); Supervision (lead); Validation (lead); Visualization (equal); Writing – original draft (supporting); Writing – review & editing (supporting). **Julien Carlier:** Conceptualization (lead); Formal analysis (equal); Funding acquisition (lead); Project administration (lead); Validation (lead); Writing – original draft (equal); Writing – review & editing (equal). **Malika Toubal:** Data curation (supporting); Investigation (supporting); Methodology (supporting); Resources (equal); Writing – original draft (supporting); Writing – review & editing (supporting). **Bertrand Nongaillard:** Conceptualization (supporting); Investigation (supporting); Methodology (supporting); Resources (equal); Validation (equal); Writing – original draft (supporting); Writing – review & editing (supporting).

DATA AVAILABILITY

The data that support the findings of this study are available from the corresponding author upon reasonable request.

REFERENCES

[1]A. Parvulescu and C. S. Clay, "Reproducibility of signal transmissions in the ocean," Radio Electron. Eng. **29**, 223–228 (1965).
[2]M. Fink, D. Cassereau, A. Derode, C. Prada, P. Roux, M. Tanter, J.-L. Thomas, and F. Wu, "Time-reversed acoustics," Rep. Prog. Phys. **63**, 1933–1995 (2000).
[3]F. Wu, J.-L. Thomas, and M. Fink, "Time reversal of ultrasonic fields. II. Experimental results," IEEE Trans. Ultrason. Ferroelectr. Freq. Control **39**, 567–578 (1992).
[4]G. Montaldo, D. Palacio, M. Tanter, and M. Fink, "Time reversal kaleidoscope: A smart transducer for three-dimensional ultrasonic imaging," Appl. Phys. Lett. **84**, 3879–3881 (2004).
[5]F. Ma, Z. Huang, C. Liu, and J. H. Wu, "Acoustic focusing and imaging via phononic crystal and acoustic metamaterials," J. Appl. Phys. **131**, 011103 (2022).
[6]V. Preobrazhensky, P. Pernod, Y. Pyl'nov, L. Krutyansky, N. Smagin, and S. Preobrazhensky, "Nonlinear acoustic imaging of isoechogenic objects and flows using ultrasound wave phase conjugation," Acta Acust. Acust. **95**, 36–45 (2009).
[7]N. Quieffin, S. Catheline, R. K. Ing, and M. Fink, "Real-time focusing using an ultrasonic one channel time-reversal mirror coupled to a solid cavity," J. Acoust. Soc. Am. **115**, 1955–1960 (2004).
[8]W. S. Gan, "Application of time-reversal acoustics to medical ultrasound imaging," in *Time Reversal Acoustics*, edited by W. S. Gan (Springer, Singapore, 2021), pp. 101–107.
[9]J. Rufo, P. Zhang, R. Zhong, L. P. Lee, and T. J. Huang, "A sound approach to advancing healthcare systems: The future of biomedical acoustics," Nat. Commun. **13**, 3459 (2022).
[10]G. Montaldo, G. Lerosey, A. Derode, A. Tourin, J. de Rosny, and M. Fink, "Telecommunication in a disordered environment with iterative time reversal," Waves Random Media **14**, 287–302 (2004).
[11]G. Lerosey, J. de Rosny, A. Tourin, A. Derode, G. Montaldo, and M. Fink, "Time reversal of electromagnetic waves and telecommunication," Radio Sci. **40**, RS6S12, https://doi.org/10.1029/2004RS003193 (2005).
[12]G. Lerosey and M. Fink, "Wavefront shaping for wireless communications in complex media: From time reversal to reconfigurable intelligent surfaces," Proc. IEEE **110**, 1210–1226 (2022).
[13]N. Chakroun, M. Fink, and F. Wu, "Time reversal processing in ultrasonic nondestructive testing," IEEE Trans. Ultrason. Ferroelectr. Freq. Control **42**, 1087–1098 (1995).
[14]C. H. Wang, J. T. Rose, and F.-K. Chang, "A synthetic time-reversal imaging method for structural health monitoring," Smart Mater. Struct. **13**, 415 (2004).
[15]N. Smagin, A. Trifonov, O. Bou Matar, and V. Aleshin, "Local damage detection by nonlinear coda wave interferometry combined with time reversal," Ultrasonics **108**, 106226 (2020).
[16]T. J. Ulrich, A. M. Sutin, T. Claytor, P. Papin, P.-Y. Le Bas, and J. A. TenCate, "The time reversed elastic nonlinearity diagnostic applied to evaluation of diffusion bonds," Appl. Phys. Lett. **93**, 151914 (2008).
[17]A. M. Sutin, J. A. TenCate, and P. A. Johnson, "Single-channel time reversal in elastic solids," J. Acoust. Soc. Am. **116**, 2779–2784 (2004).
[18]C. Draeger and M. Fink, "One-channel time reversal of elastic waves in a chaotic 2D-silicon cavity," Phys. Rev. Lett. **79**, 407–410 (1997).
[19]G. Montaldo, D. Palacio, M. Tanter, and M. Fink, "Building three-dimensional images using a time-reversal chaotic cavity," IEEE Trans. Ultrason. Ferroelectr. Freq. Control **52**, 1489–1497 (2005).
[20]B. Van Damme, K. Van Den Abeele, Y. Li, and O. B. Matar, "Time reversed acoustics techniques for elastic imaging in reverberant and nonreverberant media: An experimental study of the chaotic cavity transducer concept," J. Appl. Phys. **109**, 104910 (2011).
[21]P. Roux, B. Roman, and M. Fink, "Time-reversal in an ultrasonic waveguide," Appl. Phys. Lett. **70**, 1811–1813 (1997).
[22]A. P. Sarvazyan, L. Fillinger, and L. R. Gavrilov, "A comparative study of systems used for dynamic focusing of ultrasound," Acoust. Phys. **55**, 630–637 (2009).
[23]I. Zaaroura, M. Toubal, J. Carlier, S. Harmand, and B. Nongaillard, "Nanofluids dynamic viscosity evolution using high-frequency acoustic waves: Application applied for droplet evaporation," J. Mol. Liquids **341**, 117385 (2021).
[24]P. Chen, M. Toubal, J. Carlier, S. Harmand, B. Nongaillard, and M. Bigerelle, "Evaporation of binary sessile drops: Infrared and acoustic methods to track alcohol concentration at the interface and on the surface," Langmuir **32**, 9836–9845 (2016).
[25]A. R. Salhab, J. Carlier, P. Campistron, M. Neyens, M. Toubal, B. Nongaillard, and V. Thomy, "Polydimethylsiloxane micro-channels application for the study of dynamic wetting of nano-etched silicon surfaces based on acoustic characterization method," Solid State Phenom. **314**, 143–149 (2021).
[26]M. Davy, J. de Rosny, J.-C. Joly, and M. Fink, "Focusing and amplification of electromagnetic waves by time reversal in a leaky reverberation chamber," C. R. Phys. Propag. Remote Sensing **11**, 37–43 (2010).
[27]B. Arnal, M. Pernot, M. Fink, and M. Tanter, "Tunable time-reversal cavity for high-pressure ultrasonic pulses generation: A tradeoff between transmission and time compression," Appl. Phys. Lett. **101**, 064104 (2012).
[28]M. Hoffmann and E. Voges, "Bulk silicon micromachining for MEMS in optical communication systems," J. Micromech. Microeng. **12**, 349 (2002).
[29]J. Gao, J. Carlier, S. Wang, P. Campistron, D. Callens, S. Guo, X. Zhao, and B. Nongaillard, "Lab-on-a-chip for high frequency acoustic characterization," Sens. Actuators B **177**, 753–760 (2013).
[30]V. B. Thati, N. Smagin, H. Dahmani, J. Carlier, and I. Alouani, "Identification of ultra high frequency acoustic coda waves using deep neural networks," IEEE Sens. J. **21**, 20640–20647 (2021).
[31]H. Dahmani, I. Zaaroura, A. Salhab, P. Campistron, J. Carlier, M. Toubal, S. Harmand, V. Thomy, M. Neyens, and B. Nongaillard, "Fabrication and optimization of high frequency ZnO transducers for both longitudinal and shear

emission: Application of viscosity measurement using ultrasound," Adv. Sci. Technol. Eng. Syst. J. **5**, 1428–1435 (2020).
[32]T. Misaridis and J. Jensen, "Use of modulated excitation signals in medical ultrasound. Part I: Basic concepts and expected benefits," IEEE Trans. Ultrason. Ferroelectr. Freq. Control **52**, 177–191 (2005).
[33]M. Tanter, J.-L. Thomas, and M. Fink, "Time reversal and the inverse filter," J. Acoust. Soc. Am. **108**, 223–234 (2000).
[34]M. Tanter, J.-F. Aubry, J. Gerber, J.-L. Thomas, and M. Fink, "Optimal focusing by spatio-temporal inverse filter. I. Basic principles," J. Acoust. Soc. Am. **110**, 37–47 (2001).
[35]T. J. Ulrich, B. Anderson, P.-Y. L. Bas, C. Payan, J. Douma, and R. Snieder, "Improving time reversal focusing through deconvolution: 20 questions," Proc. Meet. Acoust. **16**, 045015 (2012).
[36]B. E. Anderson, J. Douma, T. Ulrich, and R. Snieder, "Improving spatio-temporal focusing and source reconstruction through deconvolution," Wave Motion **52**, 151–159 (2015).
[37]C. Draeger, J.-C. Aime, and M. Fink, "One-channel time-reversal in chaotic cavities: Experimental results," J. Acoust. Soc. Am. **105**, 618–625 (1999).
[38]T. Goursolle, S. Callé, S. Dos Santos, and O. Bou Matar, "A two-dimensional pseudospectral model for time reversal and nonlinear elastic wave spectroscopy," J. Acoust. Soc. Am. **122**, 3220–3229 (2007).
[39]A. Derode, A. Tourin, and M. Fink, "Ultrasonic pulse compression with one-bit time reversal through multiple scattering," J. Appl. Phys. **85**, 6343–6352 (1999).
[40]G. Montaldo, P. Roux, A. Derode, C. Negreira, and M. Fink, "Generation of very high pressure pulses with 1-bit time reversal in a solid waveguide," J. Acoust. Soc. Am. **110**, 2849–2857 (2001).
[41]T. Strohmer, M. Emami, J. Hansen, G. Papanicolaou, and A. Paulraj, "Application of time-reversal with MMSE equalizer to UWB communications," in *IEEE Global Telecommunications Conference, GLOBECOM '04* (IEEE, 2004), Vol. 5, pp. 3123–3127.